International Journal of Biological Macromolecules 307 (2025) 142357

Contents lists available at ScienceDirect

International Journal of Biological Macromolecules

journal homepage: www.elsevier.com/locate/ijbiomac

Structural determinants of mucins in influenza virus inhibition: The role of sialylated glycans and molecular size

Cosmin Butnarasu [a], Marc Safferthal [b,c], Jolly Thomas [a], Tatyana L. Povolotsky [b], Robyn Diehn [a], Kerstin Fentker [b,d], Philipp Mertins [d,e,f], Kevin Pagel [b,c], Daniel C. Lauster [a,*]

[a] Institute of Pharmacy, Biopharmaceuticals, Freie Universität, Berlin 14195, Germany
[b] Institute of Chemistry and Biochemistry, Freie Universität, Berlin 14195, Germany
[c] Fritz Haber Institute of the Max Planck Society, 14195 Berlin, Germany
[d] Max Delbrück Center of Molecular Medicine, Berlin 13125, Germany
[e] Berlin Institute of Health at Charité – Universitätsmedizin Berlin, Berlin, Germany
[f] German Center for Child and Adolescent Health (DZKJ), partner site Berlin, Berlin, Germany

ARTICLE INFO

Keywords:
Mucins
Glycomics
Influenza virus
Antivirals
H3N2

ABSTRACT

Mucins are heavily glycosylated proteins that play a crucial role in protecting mucosal surfaces against pathogens, including influenza viruses. This study investigates the antiviral properties of bovine submaxillary mucins (BSM) as a model for oral mucins against the influenza virus (A/H3N2 subtype), focusing on glycan composition and mucin size. BSM was purified, and characterized by proteomic and glycomic analysis and its antiviral efficacy was assessed after selective removal of sialic acids, *N*-glycans, or all glycans *via* enzymatic and chemical treatments. We employed virus binding and inhibition assays, including microscale thermophoresis (MST) and hemagglutination inhibition (HAI), to characterize processed mucins for structure activity correlations. Removal of sialic acids reduced BSM's antiviral activity by over 10-fold, while complete glycan removal abolished it entirely, highlighting sialylated *O*-glycans as critical for viral inhibition. *N*-glycan removal had minimal impact on antiviral efficacy. A size-dependent antiviral effect was observed: smaller mucin fragments (~50 and 330 kDa), which retained comparable *O*-glycosylation patterns, showed significantly reduced inhibition and viral binding affinity several orders of magnitude below intact BSM. These findings underscore the importance of mucin size and sialylated *O*-glycans in antiviral defense mechanisms against influenza.

1. Introduction

Influenza A (IAV) infections continue to represent a major threat to global public health and economics. Seasonal influenza infects as many as 1 billion people, making it one of the most common respiratory diseases. The World Health Organization (WHO) estimates annually 3–5 million cases of severe illness and up to 650,000 deaths worldwide [1]. Despite advances in vaccination strategies and antiviral therapies, the constant evolution of influenza viruses continues to pose challenges to effectively combat these pathogens [2].

One promising avenue for influenza prevention and treatment lies in understanding the intricate interplay between viral components and host factors during the initial steps of infection [3]. Among these host factors, mucins, a family of heavily glycosylated proteins, represents a pivotal players in the defense against viral infections [4–6]. As the main constituents of mucus, mucins provide protection by acting as both physical and chemical barriers to pathogens while maintaining the hydration of mucosal surfaces. The core protein is rich in serine and threonine, which can carry *O*-glycans and can make up to 80 % of the mass of the protein. This extensive glycosylation gives mucins their characteristic bottlebrush-like structure, which is flexible and negatively charged overall [7].

In the initial stage of host cell infection, the viral hemagglutinin (HA) mediates the binding to sialic acid (SA) on the cell surface in a multivalent fashion, which leads to uptake of the virus particle into host cells (Fig. 1a) [8–10]. *N*-acetylneuraminic acid (Neu5Ac) and *N*-glycolylneuraminic acid (Neu5Gc) are the two major forms of SA relevant for influenza infections. While Neu5Ac is the predominant form in humans, Neu5Gc is found in other animals, such as cows and pigs [11]. Most human-adapted influenza viruses, including H1N1 and H3N2 strains,

* Corresponding author.
E-mail address: daniel.lauster@fu-berlin.de (D.C. Lauster).

https://doi.org/10.1016/j.ijbiomac.2025.142357
Received 11 January 2025; Received in revised form 3 March 2025; Accepted 19 March 2025
Available online 20 March 2025
0141-8130/© 2025 The Authors. Published by Elsevier B.V. This is an open access article under the CC BY-NC-ND license (http://creativecommons.org/licenses/by-nc-nd/4.0/).

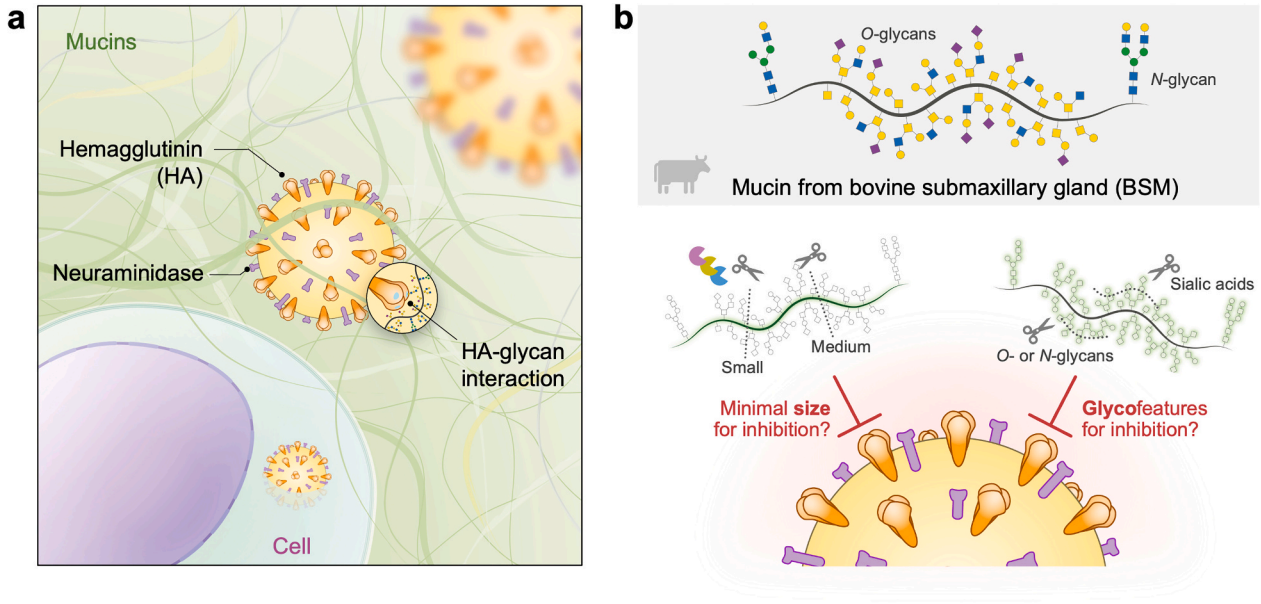

Fig. 1. Mucins in the lungs play an important role as a barrier to viral infections such as influenza A virus (IAV). (a) The glycans on mucins act as decoy receptors for IAV hemagglutinin binding, reducing the probability of epithelial cell infections. (b) Schematic illustration of the approach used in this study to explore the effect of glycans and the size of the mucin from bovine submaxillary gland on the binding to IAV.

preferentially bind to Neu5Ac, while animal-adapted virus strains can bind also Neu5Gc, which is not present in humans. An earlier study found that Neu5Gc acts as a decoy receptor for such IAV strains, but does not permit cell entry [12]. Although the mucus mesh size of approximately 120 nm permits influenza virus penetration, the highly abundant SA on mucins restricts viral diffusion [13]. Mucins, in fact, display SA as part of *N*- and *O*-glycans, and most probably they have evolved SA as a decoy for viruses to get them trapped in mucus, thereby preventing cell infection [14].

It is clear that mucins are multifunctional macromolecules, which fulfill besides antiviral properties also many more [15]. A defining characteristic of mucins that shapes their mechanical and functional properties is their remarkable size. Mucin monomers can extend up to 500 nm in length [16], forming an intricate, three-dimensional network that sterically shields viral particles while multivalently presenting SA residues. This structural organization is particularly effective against influenza viruses, as HA binding requires an optimal spacing of ~4.5 nm for intra-trimeric interactions and up to 14 nm for inter-trimeric binding [17,18]. In principle, the extended size and network formation of mucins allow them to meet these spatial criteria, enhancing their ability to bind and trap viral particles. This natural defense mechanism has inspired the design of synthetic biopolymers to inhibit viral infections mimicking the multivalent presentation of sialic acids on the host cell surface to block virus binding [19–21]. Efforts to elucidate the impact of polymer structure on the inhibitory effect have shown, for instance, that linear polymers are superior to dendritic in inhibiting the influenza virus, highlighting the critical influence of polymer architecture [18]. However, replicating the complex glycosylation patterns of natural mucins remains a significant challenge in synthetic chemistry [22], as well as in recombinant biology [23]. Despite these advances, the size-dependent antiviral properties of natural mucins and their underlying biophysical mechanisms have yet to be systematically explored.

Here, we address the question of mucin's antiviral activity by focusing on bovine submaxillary gland mucins (BSM). We selected BSM for its abundance of both Neu5Ac and Neu5Gc, with a predominance of Neu5Ac [24,25]. To dissect the contribution of different glycan structures and size in antiviral activity, we employed enzymatic and chemical methods for selective glycan removal (horizontal cleavage), and a pool of proteases to cleave the peptide backbone (vertical cleavage), generating mucin fragments of varying size (Fig. 1b). By combining multiple enzymatic and glycan removal strategies we systematically evaluate the role of sialylation, glycan density, and molecular size, highlighting structure-function relationship. We then investigate the inhibition properties and binding to the whole virus of the horizontally and vertically cleaved mucin derivatives on IAV. We anticipate that size plays a dominant role on viral inhibition while sialylated *O*-glycans are key factors for antiviral binding.

2. Experimental section

2.1. Mucin purification

Mucin from the bovine submaxillary gland (BSM) was obtained from Sigma-Aldrich (Type I—S) as a lyophilized powder. The BSM purification protocol was adapted from a previously published method [26]. In short, BSM was dissolved at a concentration of 10 mg/mL in phosphate-buffered saline (Dulbecco's phosphate-buffered saline (DPBS) pH 7.4, without calcium and magnesium, Carl Roth), supplemented with sodium chloride at a concentration of 2 M, and stirred overnight at 4 °C. The insoluble fraction was removed by centrifugation (10,000 xg, 4 °C, 15 min). Subsequently, the mucins were isolated by size exclusion chromatography (SEC) using an Äkta Pure system (Cytiva, Germany) equipped with a HiPrep 26/60 column packed with Sephacryl 400 HR (Cytiva, Germany) and a bed volume of 318.6 mL. DPBS (pH 7.4) supplemented with 2 M sodium chloride was used as equilibration and elution buffer. Approximately 5 mL of the BSM sample was loaded into the column. The loading flow rate was 1 mL/min while the elution flow was set at 0.5 mL/min. Sample elution was recorded by monitoring absorbance at 280 and 214 nm. Fractions of 40 mL were pooled and concentrated by centrifugation filtering (100 kDa MWCO Vivaspin® Turbo 15, Sartorius) and analyzed by periodic acid-Schiff (PAS) reaction to monitor the fractions containing glycosylated material. The concentrated sample was resuspended three times in Milli-Q water to remove the excess salts. The sample was then lyophilized and stored at −80 °C until further use.

2.2. Proteomic analysis

Crude BSM (#SLCK8402) and three replicates of purified BSM were dissolved in PBS (pH 7.4, without calcium and magnesium) at a concentration of 2 mg/mL. Sample preparation was performed as described by Rulff et al. [27]. Briefly, 50 μL of the solution was reduced and alkylated by the addition of SDS buffer (2 % *w/v* SDS, 50 mM Tris-HCl pH 8, 0.5 mM EDTA, 75 mM NaCl, 10 mM DTT, 40 mM chloroacetamide final concentration) and incubated at 95 °C for 10 min. After cooling, Benzonase® (10.25 U, Merck) was added and incubated for 15 min at room temperature. The protein sample was purified using a single-pot, solid-phase enhanced sample preparation (SP3 clean-up) [28]. Proteins were then incubated for 1 h with peptide N-glycosidaseF (PNGase F) - 500 U, New England Biolabs - to remove N-glycosylation, followed by overnight digestion with sequence-grade trypsin (Promega) and lysyl endopeptidase (LysC, Wako) (1:50 enzyme:substrate ratio, 37 °C). Trifluoroacetic acid was added to a final concentration of 1 % (*v*/v) to stop the digestion. Peptides in the supernatant were desalted using C18 stage tips [29]. The eluted and dried peptides were reconstituted in 10 μL of 3 % (*v*/v) acetonitrile (ACN) with 0.1 % (*v*/v) formic acid (FA). 2 μL of peptides were separated on a Vanquish Neo UHPLC system on a reversed-phase column (20 cm fritless silica microcolumns with an inner diameter of 75 μm, in-house packed with ReproSil-Pur C18-AQ 1.9 μm resin (Dr Maisch GmbH)). The gradient length was 98 min at a flow rate of 250 nL/min. The buffer B (90 % (v/v) ACN, 0.1 % (v/v) FA) concentration was increased from 2 % to 60 %.

The separated peptides were analyzed on an Orbitrap Exploris 480 mass spectrometer (Thermo Fisher Scientific) in data-dependent acquisition (DDA) mode. At MS1 level, the resolution was 60 k with a normalized AGC target of 300 % and a maximum injection time of 10 ms. For MS2 scans, the top 20 ions were selected with a dynamic exclusion time of 30 s. Ions were measured at 15 K resolution with an AGC target of 100 % and a maximum injection time of 22 ms.

MaxQuant (V 2.0.3.0) was used for database searching (Uniprot database: bovine proteins (downloaded 2022–09)) [30]. Variable modifications were defined as oxidation (M), *N*-terminal acetylation and deamidation (N, Q), and carbamidomethyl (C) were defined as fixed modifications. In addition, "match between runs", label-free quantification, and iBAQ algorithms were used. The mass spectrometry proteomics data have been deposited to the ProteomeXchange Consortium *via* the PRIDE partner repository with the dataset identifier PXD054384. R (V 4.2.2) was used for statistical analysis. First, proteins were filtered for 'reverse' and 'identified by site only'. Proteins identified as "potential contaminants" were only filtered if they were not from bovine databases. Only proteins quantified in 2 of the 3 purified samples and in the crude BSM sample were considered for further analysis. Statistical analysis was performed using one-sided moderated *t*-test using the limma-package [31]. The Benjamini-Hochberg method, contained in the same package, was used for multiple comparison correction.

2.3. Glycan removal from mucins

N-linked glycans were removed by treatment with PNGase-F enzyme (New England Biolabs) according to the manufacturer's instructions. Briefly, purified mucin (1 mg/mL) was incubated with PNGase-F (50,000 U/mL) in 5 mM sodium phosphate, pH 7.5, at 37 °C for 24 h. After deglycosylation, the enzyme was inactivated by heating at 75 °C for 10 min. The sample was concentrated, and the cleaved *N*-linked glycans were removed by three cycles of centrifugation filtering (50 kDa MWCO Amicon Ultra-4). The structure of the filtered *N*-glycans were further analyzed (see Section 2.6)

Desialylated mucin was prepared by incubation of purified mucin with SialEXO® (G1-SM1–020, Genovis) according to the manufacturer's instructions. Shortly, 1 μg of purified mucin was incubated with 1 unit of SialEXO® at 37 °C overnight in 20 mM Tris HCl buffer, pH 6.8. The cleaved sialic acid was removed by three cycles of centrifugation filtering (100 kDa MWCO Amicon Ultra-4).

Unspecific deglycosylation was performed following a previously published protocol consisting of oxidation and β-elimination [32]. Briefly, a 10 mg/mL of purified BSM sample was solubilized in 0.33 M NaCl at 4 °C overnight. Acetic acid was added to 0.1 M, and the pH was adjusted to 4.5 with 1 M NaOH. The oxidation was started by adding ice-cold 200 mM $NaIO_4$ to a final concentration of 100 mM $NaIO_4$. The solution was left to stand in the dark at 4 °C overnight. Next, the unreacted periodate was destroyed by adding ½ volume of 400 mM $Na_2S_2O_3$/100 mM NaI/100 mM $NaHCO_3$ (in a 1:1:1 volume ratio). The elimination was started by adding 1 M NaOH to pH 10.5. After standing for 1 h in the cold while maintaining the pH, the solution was dialyzed (100 kDa MWCO) at 4 °C against water. The sample was then lyophilized and stored at −80 °C until further use.

2.4. Enzymatic mucin fragmentation

For all the digestion reactions, mucin was first denatured, reduced, and alkylated before protease treatment. Purified mucin was dissolved at a concentration of 50 mg/mL in 6 M guanidinium hydrochloride and 5 mM DTT at 37 °C under mild agitation for 1 h. Then, the sample was alkylated with 20 mM iodoacetamide at room temperature in the dark for 30 min. After alkylation, the sample was diluted with 50 mM Tris HCl buffer until the concentration of guanidinium hydrochloride reached 0.3 M. Instead of Tris buffer, 40 mM HCl, pH 2, was used in the reaction with pepsin (Promega, V1959). To increase protease efficiency, specific adjustments were made to the pH and the composition of the Tris buffer. In particular, *Serratia marcescens* enzyme (SmE) and secreted protease of C1 esterase inhibitor (StcE) digestions were carried out at pH 8, supplemented with 2 mM $ZnCl_2$; ficin (Merck, F4165), bromelain (Merck, B4882), and papain (Merck, 1.07144) digestions were performed at pH 7, supplemented with 2 mM cysteine; trypsin (Merck, T1426) and chymotrypsin (Merck, C4129) digestions were conducted at pH 8, with the addition of 10 mM $CaCl_2$; finally, elastase (Promega, V1891) and proteinase K (Merck, 124,568) digestions were carried out at pH 9 and pH 8, respectively. All the proteases were added in a 1:20 protease:BSM ratio, and the digestion was conducted at 37 °C overnight. The reaction was quenched by adding Protease Inhibitor Cocktail (Abcam, ab271306) in a 1:100 volume ratio.

2.5. Isolation and purification of mucin fragments

Mucin fragments obtained from the proteinase K digestion were enriched and purified by size exclusion chromatography using an Äkta Pure system (Cytiva, Germany) equipped with a Superdex 200 Increase 10/300 GL prepaked column (Cytiva, Germany). DPBS (pH 7.4) was used as equilibration and elution buffer. Approximately 500 μL of the digested sample were loaded into the column. The loading flow rate was 0.75 mL/min while the elution flow was set at 0.25 mL/min. Mucin fragments obtained from StcE digestion were enriched and purified by affinity chromatography using the same FPLC system equipped with a HisTrap HP 1 mL column (Cytiva, Germany). 20 mM Tris buffer (pH 8.0) containing 25 mM imidazole and 500 mM NaCl was used as loading and washing buffer while the same buffer at 500 mM imidazole concentration was used for the elution phase. Approximately 2 mL sample volume was applied at 0.1 mL/min and eluted at 1 mL/min. Sample elution was recorded by monitoring absorbance at 280 and 214 nm.

Fractions of 2 mL were pooled and concentrated by centrifugation filtering (10 kDa MWCO Vivaspin® Turbo 15, Sartorius) and analyzed by PAS reaction to monitor the fractions containing glycosylated material. The concentrated sample was resuspended three times in Milli-Q water to remove the excess salts. The sample was then lyophilized and stored at -80 °C until further use.

SDS-PAGE/PAS was used to analyze the molecular weight of the mucin fragments, and the hydrodynamic radius in DPBS was measured

by dynamic light scattering (DLS) using a Nanotemper Prometheus Panta device.

Sialic acid was measured using the NANA assay (MAK314, Sigma-Aldrich) where sialic acid is oxidized to formylpyruvic acid which reacts with thiobarbituric acid to form a pink colored product.

2.6. Structural analysis of O- and N-glycans

O-glycans from intact purified BSM (2 mg/mL in H_2O) and digested BSM fractions (2 mg/mL in H_2O) were released by reductive β-elimination [33]. 80 μL of each sample were incubated with 0.5 mM NaOH (10 μL) and 5 M $NaBH_4$ (10 μL) at 50 °C for 16 h. Reactions were quenched with acetic acid (15 μL). The solutions were desalted on 400 mg Dowex 50WX8 cation exchange beads (Sigma-Aldrich, USA). Prior to sample loading, the resin was washed with MeOH (3 × 1 mL), and conditioned with 1 M HCl (1 mL), MeOH (1 mL) and H_2O (1 mL). Samples were loaded on the resin and eluted with H_2O (2 × 500 μL). Glycans were extracted using 50 mg Hypercarb SPE cartridges (Thermo Fischer, USA). Cartridges were conditioned with ACN 0.1 % (*v*/v) TFA (1 mL), and 0.1 % TFA in H_2O. Glycans were loaded on the cartridge and washed with 0.1 % TFA in H_2O (3 × 1 mL). Glycans were eluted with 50 % ACN 0.1 % TFA (4 × 100 μL) and dried in a SpeedVac.

The collected *N*-glycans (see Section 2.3) were lyophilized and subsequently redissolved in 1 M $NaBH_4$ (100 μL). The reaction mixture was incubated at 50 °C for 3 h. The reaction mixture was quenched with acetic acid (25 μL). The solution was desalted on 400 mg Dowex 50WX8 cation exchange beads (Sigma-Aldrich, USA). Prior to sample loading, the resin was washed with MeOH (3 × 1 mL), and conditioned with 1 M HCl (1 mL), MeOH (1 mL) and H_2O (1 mL). The sample was loaded on the resin and eluted with H_2O (2 × 500 μL). Glycans were extracted using 50 mg Hypercarb SPE cartridges (Thermo Fischer, USA). Cartridges were conditioned with ACN 0.1 % TFA (1 mL), and 0.1 % TFA in H_2O. Glycans were loaded on the cartridge and washed with 0.1 % TFA in H_2O (3 × 1 mL). Glycans were eluted with 50 % ACN 0.1 % TFA (4 × 100 μL) and dried in a SpeedVac.

PGC-LC-MS/MS were performed using a SYNAPT G2-Si spectrometer (Waters, U.K.) equipped with an Acquity UPLC system. The glycan alditols were redissolved in 40 μL and 5 μL were injected. Glycan alditols were separated using a 100 × 2.1 mm I.D. PGC column of 5 μm particle size (Hypercarb, Thermo Scientific, U.S.A.) with a linear gradient from 0 to 40 % ACN in 10 mM NH_4HCO_3 at room temperature at a flow rate of 150 μL/min over 40 min. Analytes were ionized *via* electrospray ionization in negative ion mode with a capillary voltage of 2.8 kV and a source temperature of 150 °C. Fragmentation *via* collision-induced dissociation was performed using collision energy ramps (15 to 120 eV) dependent on the *m/z* of the precursor ion. The MassLynx software (version 2.0.7, Waters) was used for data acquisition and processing. Chromatograms were deconvoluted and integrated with MZmine 3 [34]. Glycan structures were manually identified from MS/MS spectra based on diagnostic fragment ions [35,36] using GlycoWorkBench 2.1 [37].

2.7. Expression and purification of mucinases

The pET28b-StcE_Δ35-NHis plasmid was supplied by the Carolyn R. Bertozzi lab (Stanford University) with permission from Natalia Strynadka (University of British Columbia), where the plasmid was originally created. The expression and purification were carried out with Junqioa Jia in the Markus Wahl lab (Freie Universität Berlin). The pET28b-StcE_Δ35-NHis plasmid was transformed using electroporation into electrocompetent *E. coli* BL21(DE3) cells in the presence of 50 μg/mL kanamycin. Bacterial cell culture was produced from a single colony and grown at 37 °C, shaking, until an OD_{600} of 0.8, when it was induced with 1.5 mL of 0.2 mM IPTG for 1 L of cell culture. The bacterial cell culture was then placed in a shaking incubator at 18 °C and grown overnight. From this point, the bacterial cells are kept continuously on ice or at 4 °C conditions. The culture was spun down, supernatant discarded and two complete Mini EDTA-free protease inhibitor cocktail tablets (Roche) were added to 20 mL concentrated bacterial cell pellet and resuspended in 50 mL lysis buffer (20 mM HEPES pH 7.5, 500 mM NaCl) and lysed using Sonopuls Ultrasonic Homogenizer HD (Bandelin) with 65 % amplitude for 25 min. The lysed cells were centrifuged at 21,500 x*g* at 4 °C for 60 min. The supernatant was kept for StcE protein purification using the Äkta Pure FPLC system and the HisTrap HP column (GE Healthcare Life Sciences). Washing with 20 column volumes (CV) of lysis buffer plus 20 mM imidazole, the protein was eluted using a linear gradient from 20 mM to 250 mM imidazole over the course of 20 min. StcE protein expression was confirmed *via* SDS-PAGE and StcE-containing fractions were pooled and then concentrated using Amicon Ultra 30 kDa MWCO filters (Millipore Sigma). The protein was further purified using size exclusion chromatography (SEC) FPLC HiLoad Superdex™ S200 16/60 column (GE Healthcare) equilibrated with DPBS buffer. Purified fractions as identified by SDS-PAGE were pooled and again then concentrated using Amicon Ultra 30 kDa MWCO filters (Millipore Sigma). Purified and concentrated StcE was then flash-frozen in liquid nitrogen and stored at −80 °C.

For protein expression of SmEnhancin (SmE), *E. coli* BL21-CodonPlus (DE3)-RIPL was transformed with pET28a_SmE, which was kindly gifted by Stacy A. Malaker (Yale University), and streaked out on LB agar plates (kanamycin 50 μg/mL, chloramphenicol 34 μg/mL, streptomycin 50 mg/mL). One colony was picked and grown in LB medium (50 μg/mL kanamycin, 34 μg/mL chloramphenicol, 50 mg/mL streptomycin) at 250 rpm, 37 °C, overnight. With this preculture, TB AIM medium (20 mM glucose, 50 μg/mL kanamycin, 34 μg/mL chloramphenicol, 50 mg/mL streptomycin) was inoculated at an OD_{600} of 0.03, grown at 250 rpm, 37 °C, and the exponentially growing culture was aliquoted at an OD_{600} of 2.67 (including 7 % DMSO) and snap-frozen in liquid nitrogen. TB AIM medium (30 mM lactose, 11,25 g/L glycerol, 50 μg/mL kanamycin, 17 μg/mL chloramphenicol) was inoculated with an OD_{600} of 0.04 of the thawed bacterial stock and grown at 25 °C, 250 rpm grown for 23 h. The culture was harvested and washed two times with lysis buffer (50 mM HEPES, 200 mM NaCl, 2.5 mM $CaCl_2$, 2.5 mM $MgCl_2$, pH 8.0) by centrifugation at 4000 x*g* for 10 min. The lysis of a bacterial pellet of 100 mL bacterial culture was performed with 2.5 % (*v*/v) DMSO, 2,5 % (v/v) n-propanol, 30 mM N-lauroylsarcosine, 1:100 protease inhibitor (Halt™ Protease Inhibitor Cocktail, EDTA-free (100×)) in lysis buffer (total volume 46 mL) at 50 % intensity, 50 % cycle for 15 min (Sonopuls HD 2200 with sonotrode MS73 by Bandelin). The lysate was centrifuged at 12.000 x*g* for 30 min and filtered through a 0.2 μM PES filter and stored on ice for further use.

The protein was purified using an ÅKTA Pure FPLC (Cytiva) with HisTrap column (Cytiva) following a previously published protocol [38].

2.8. Gel electrophoresis and blotting

Samples were analyzed by sodium dodecyl sulfate polyacrylamide gel electrophoresis (SDS-PAGE). The samples were mixed with 4× loading dye in a ratio of 3:1 and then thermally denatured at 95 °C for 5 min. The mixture was briefly centrifuged, and 10 μL were loaded onto a precast polyacrylamide gel (4–20 % Mini-PROTEAN® TGX™, Bio-Rad). Additionally, 5 μL of a prestained protein standard solution (ProSieve QuadColor Protein Marker, 4.6–300 kDa, Lonza) was loaded on a separate lane. The gel was run at 100 V in SDS running buffer (25 mM Tris base, 200 mM glycine, 0.1 % *w*/*v* SDS) for 80 min.

After the run, the gel was rinsed with water to remove the excess SDS running buffer, and the gel was subjected to PAS staining for glycan detection as previously reported [39]. First, the gel was fixed in 25 % (*v*/v) MeOH and 10 % (v/v) acetic acid for 1 h under gentle shaking. Then, the gel was washed in water for 20 min. Oxidation was performed in a 2 % periodic acid solution at room temperature for 15 min and washed twice with water for 2 min. The oxidized gel was stained with Schiff reagent at room temperature, protecting from light, for 40 min. The

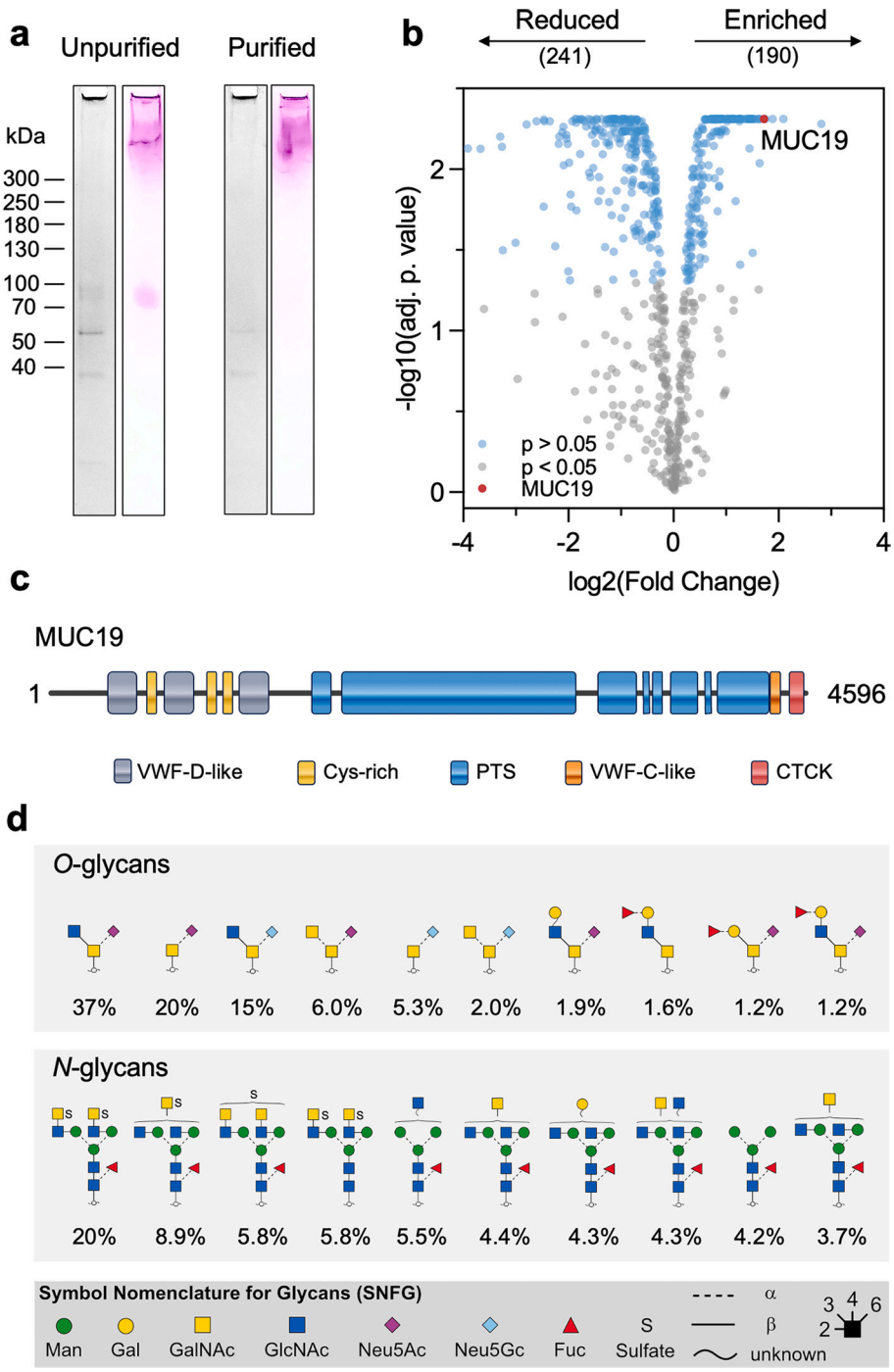

Fig. 2. Purification of bovine submaxillary mucin (BSM) by size exclusion chromatography (SEC) enriches the mucin content. (a) SDS-PAGE stained with Coomassie blue (black and white) and periodic acid-Schiff (colored) of BSM before and after SEC purification. (b) Volcano plot of proteins with significantly different intensities (adjusted *p*-value <0.05, moderated *t*-test) highlighted in blue. Mucin 19 (MUC19) is highlighted in red. On top of the plot are reported the number of proteins which abundance was reduced (241) and enriched (190) after purification. (c) Scheme of the structure of the gel forming bovine MUC19 based on the Uniprot entry P98091. (d) Putative structures and relative abundance of the top-10 of *O*- and *N*-glycans identified in the purified BSM.

unreacted Schiff reagent was removed by washing the gel with 1 % sodium metabisulfite until a clear background was observed. The gel was rinsed with water and imaged with ChemiDoc XRS (BioRad). Proteins detection was achieved using either Der Blaue Jonas solution (GRP, Germany), or silver staining.

The efficiency of enzymatic desialylation and *N*-glycan removal from mucin was verified by lectin blotting. After separation on SDS-PAGE, samples were transferred to nitrocellulose membrane (Carl Roth, GmbH) using a Trans-Blot® Turbo™ Transfer System (Bio-Rad). The membrane was blocked with 3 % bovine serum albumin (BSA) in PBST at 4° overnight, washed, and incubated with fluorescently labeled lectins at room temperature for 1 h. Concanavalin A FITC conjugate (Merck) and wheat germ agglutinin Alexa 647 conjugate (ThermoFisher Scientific) were used to specifically stain *N*-linked glycans and sialic acid, respectively. The specificity of the lectin binding was tested using untreated mucin as a positive control, while bovine serum albumin was used as the negative control.

The unpurified and purified mucins were also analyzed using agarose

gel electrophoresis and stained by PAS as previously described [40,41].

2.9. Hemagglutination inhibition assay

Hemagglutination inhibition assay was conducted using A/Panama/2007/1999 (H3N2) virus as previously described [18]. First, the virus was titrated for the hemagglutination assay (HA). Shortly, 50 μL virus concentrate was serially diluted twofold in DPBS using 96-well plates. Then, 50 μL of 1 % human red blood cells (German Red Cross, Berlin) were added to each well and incubated at room temperature for 60 min. The HA unit (HAU) per 50 μL of virus solution was identified as the last well showing hemagglutination.

The hemagglutination inhibition assay (HAI) was conducted by incubating the virus with human red blood cells to yield agglutination and concentration-dependent inhibition of agglutination (*i.e.*, without and with an agglutination inhibitor). The compounds (*i.e.*, mucin-derived samples) were two-fold serially diluted in DPBS (pH 7.4, without calcium and magnesium), and 4 HAU were added to all wells. The virus and the compounds were incubated at room temperature for 30 min to reach equilibrium. After incubation, 50 μL of 1 % human red blood cells were added. The plate was gently tapped and further incubated at room temperature for 1 h. The lowest inhibitor concentration necessary to achieve complete inhibition of agglutination is defined as the inhibitor constant (K_i^{HAI}); this was determined by analysis of the plate after 1 h of incubation and was expressed as the total dry mass of the compound per volume (μg/mL).

2.10. Microscale thermophoresis

Binding measurements of the influenza virus were carried out by microscale thermophoresis (MST) using a Monolith NT.115 (Nanotemper) from the Heberle lab (FU Berlin). The envelope of a 1 mg/mL (expressed as protein content) suspension of A/X31/1 (A/Aichi/1968 (H3N2) reassorted with A/Puerto Rico/8/1934 (H1/N1)) virus was labeled with 20 μM octadecyl rhodamine B (R18, Invitrogen), under gentle shaking on ice for 30 min. Unbound R18 was removed using desalting columns (Zeba™7 K MWCO, Thermo Scientific). The collected virus was filtered using a 0.45 μm filter to remove virus aggregates. As a quality control, the amount of virus and its binding ability were tested by performing a hemagglutination assay. All MST measurements were carried out at 22 °C in premium capillaries using default settings (initial fluorescence = 5 s, thermophoresis = 30s, and recovery = 5 s). The MST power was set at 20 % and the LED power (green LED) at 80 %. For affinity measurement, the ligands were serially diluted 1:2 in DPBS and mixed with R18-labeled virus (4 HAU, C final ~0.1 nM virus particles). The obtained data for the mucin building block was analyzed with a gating strategy 1.5 s after the start of the thermophoresis, and fitted as previously shown [18]. The data obtained for intact mucin was analyzed based on the initial fluorescence and fitted according to the bleaching rate, as previously shown [42].

2.11. Statistical analysis

The statistical analysis was performed with GraphPad Prism 10 software. All data were presented as mean ± SD. Unless elsewhere stated, statistical difference was determined with Student's *t*-test (****, $p < 0.0001$; ***, $p < 0.001$; **, $p < 0.01$; $p < 0.05$; and ns, $p > 0.05$). Kruskal-Wallis test followed by Dunn's multiple comparison test was used to account for the non-parametric data and compare multiple groups assuming a non-normal distribution.

3. Results

3.1. Purification and characterization of bovine submaxillary mucin

BSM is a commercially available mucin frequently used in biomaterial and biomedical applications [6,13,27]. Due to the presence of sialylated glycans, it represents a suitable oral mucin model for interaction studies with pathogens, such as IAV. However, one of the major drawbacks of commercial mucins is their lack of purity. Due to harsh processing, commercial mucins often contain numerous contaminants, such as endogenous proteases, small molecules, and processing additives, that can compromise their efficacy in various biological applications [43,44]. Aiming to minimize the effect of these contaminants, we purified BSM by size exclusion chromatography (Fig. S1a) by modifying a protocol previously used for the purification of porcine gastric mucins [26].

A qualitative analysis of the purity of BSM after purification was checked by gel electrophoresis. To better appreciate variations in the high molecular weight region, we first conducted agarose gel electrophoresis. We observed that after purification, the band at an apparent molecular weight of ~500 kDa, corresponding to either mucin fragments or glycosylated contaminants, was strongly reduced (Fig. S1b). Differences in the smaller molecular weight region were visualized by SDS-PAGE. Here, multiple distinct bands below 100 kDa were visible in the unpurified product using both glycan and protein staining; on the contrary, after size exclusion chromatography purification, the same bands were completely or partially removed (Fig. 2a). By that way, mucin content was increased, which became obvious from a lower protein and a higher carbohydrate content (Fig. S1c, d). The higher carbohydrate content measured as PAS signal in samples at the same concentration of dry weight per volume points to an enrichment of the mucin fraction after purification. Distinct changes in composition between the crude and the purified BSM were revealed also by proteomic analysis (Fig. 2b). Initially, 697 proteins were identified in the crude BSM; this number was reduced to around 660 proteins after purification (for complete list see Supplementary Data). Many of the remaining proteins (241) were significantly, and up to 16-times, reduced in their abundance after purification. The only type of mucin detected was the gel-forming MUC19 (Fig. 2c), which shares similar domain organization and structural features with other secreted mucins such as MUC2, MUC5AC, MUC5B, and MUC6 [45,46]. Sequence alignment of bovine MUC19 (Uniprot P98091) with human MUC19 (Uniprot Q7Z5P9) reveals a 54 % identity, highlighting substantial conservation between the two species. Notably, the proportion of MUC19 in the purified BSM product increased approximately threefold, from around 3.5 % to about 11 %. It is worth mentioning that for the quantification of MUC19 content we used the iBAQ algorithm to quantify absolute intensities. Even though the relative quantification is very robust with a large number of identified peptides, iBAQ values may underestimate absolute mucin levels as not all theoretical tryptic peptides can be measured. The highly glycosylated regions of mucins are highly resistant to proteolytic cleavage (*vide infra*), making detection of peptides in these regions challenging and thereby reducing the reported intensities.

N- and *O*-glycosylation of the purified BSM was analyzed by PGC-LC-MS/MS. A total of 40 *O*- and 24 *N*-glycans were identified (for complete assignment see Supplementary Data) and the top-10 most abundant structures are reported in Fig. 2d. The top-10 most abundant *O*-glycan structures make up >90 % of the BSM *O*-glycosylation. The identified *O*-glycans consisted of di- to heptasaccharides, however, >85 % (expressed as relative abundance) of the *O*-glycans consist of small structures not larger than trisaccharides. As reported in previous studies, sialic acid units were found on 22 (93 %) *O*-glycans, including 12 structures (69 %) with Neu5Ac and 10 structures (24 %) with Neu5Gc [24]. The majority of the sialic acid units are α2–6 linked (Fig. S2) to the core GalNAc. Additionally, 20 structures (9 %) carry one or more fucose units mostly at the terminal ends of the *O*-glycans. The majority of the *O*-glycan structures originate from core 3 (GlcNAcβ1–3GalNAc) with 57 % and the Tn antigen (GalNAc) with 25 %. The remaining *O*-glycans are based on core 1 (Galβ1–3GalNAc), 2 (Galβ1–3(GlcNAcβ1–6)GalNAc), 4 (GlcNAcβ1–3(GlcNAcβ1–6)GalNAc) and core 5 (GalNAcα1–3GalNAc). Among the identified *N*-glycans, 89 % are complex-type, biantennary *N*-

Table 1
Methods employed to selectively remove sialic acid or *O*- and *N*-linked glycans and their detection methods.

Glycan type	Removal method	Detection method
Sialic acid	Enzymatic – Sialidases derived from *Akkermansia muciniphila*	Lectin – Wheat germ agglutinin (WGA)
N-linked glycans	Enzymatic – PNGase-F	Lectin – Concanavalin A (ConA)
Unspecific (*O*- and *N*-linked glycans)	Chemical – Oxidation and β-elimination	Periodic acid – Schiff stain

glycans. Similar to previous studies, we found that the *N*-glycans of BSM are low in sialic acids but high in sulfates and core fucoses [47]. Specifically, 11 structures (57 %) are singly or doubly sulfated and 18 (83 %) are fucosylated. Based on the glycan analysis, we conclude that both *N*- and *O*-glycosylation introduce a high density of negative charges to BSM. Besides their water-binding and gel-forming properties, sialylation, sulfation and fucosylation of the glycans may further provide multiple potential interaction sites for pathogens. Although BSM does not fully replicate the diversity of human airway mucus regarding glycosylation patterns, its abundant expression of sialyl-Tn antigen makes it acting as decoy receptors for viruses. This similarly supports its role as a simplified but biologically relevant model for viral trapping.

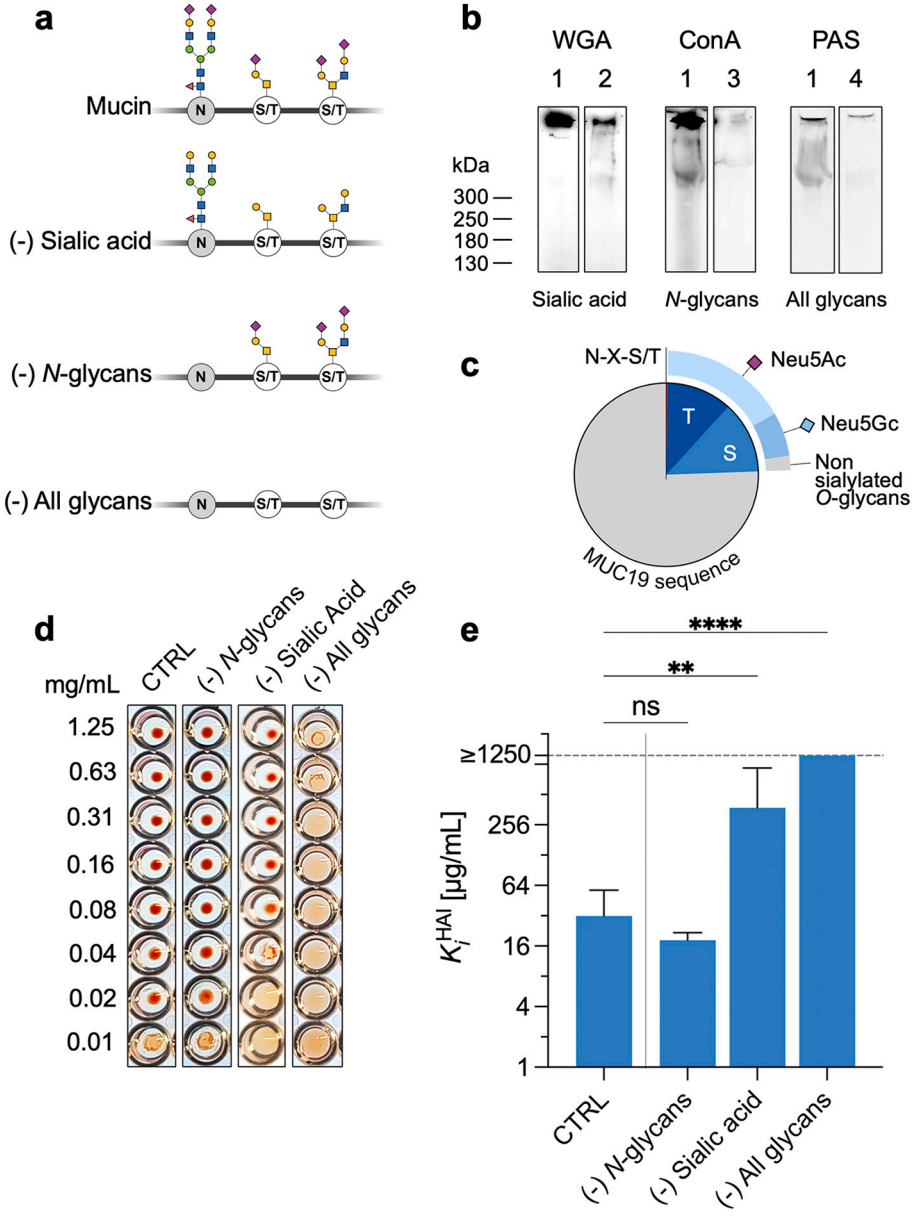

Fig. 3. Investigation of the antiviral activity of mucin after selective removal of glycans. (a) Cartoon depicting the strategy pursued for selective removal of glycans from mucin. (b) SDS-PAGE / PAS and lectin blots for selective glycans staining (1 = untreated BSM, 2 = BSM after sialic acid removal, 3 = BSM after *N*-linked glycans removal, 4 = BSM after oxidation/β-elimination). (c) Pie chart with the abundance of predicted glycosylation on asparagine (N), threonine (T), and serine (S) in the bovine MUC19 (Uniprot entry P98091). The slice of the external pie chart reports the percentage of sialylated *O*-glycans (splitted in Neu5Ac and Neu5Gc) according to the glycomic analysis of BSM. (d) Hemagglutination inhibition assay using A/Panama/2007/1999(H3N2) virus ($N = 8$, except $N_{CTRL} = 15$). (e) Bar plot of the lowest log2 inhibitor concentration necessary to achieve complete inhibition of hemagglutination caused by the virus. No antiviral effect is observed for the sample underwent ox/β elimination (without *O*- and *N*-glycans), therefore the K_i^{HAI} is set at the maximum concentration tested (*i.e.*, 1250 µg/mL). Intact purified BSM was used as control (CTRL). The significance for each group was calculated using the Kruskal-Wallis test. Results are displayed as the average (± SD) of $N \geq 3$ measurements. Results were compared by Dunn's multiple comparison test. $p < 0.05$ (*), $p < 0.01$ (**), $p < 0.001$ (***), $p < 0.0001$ (****).

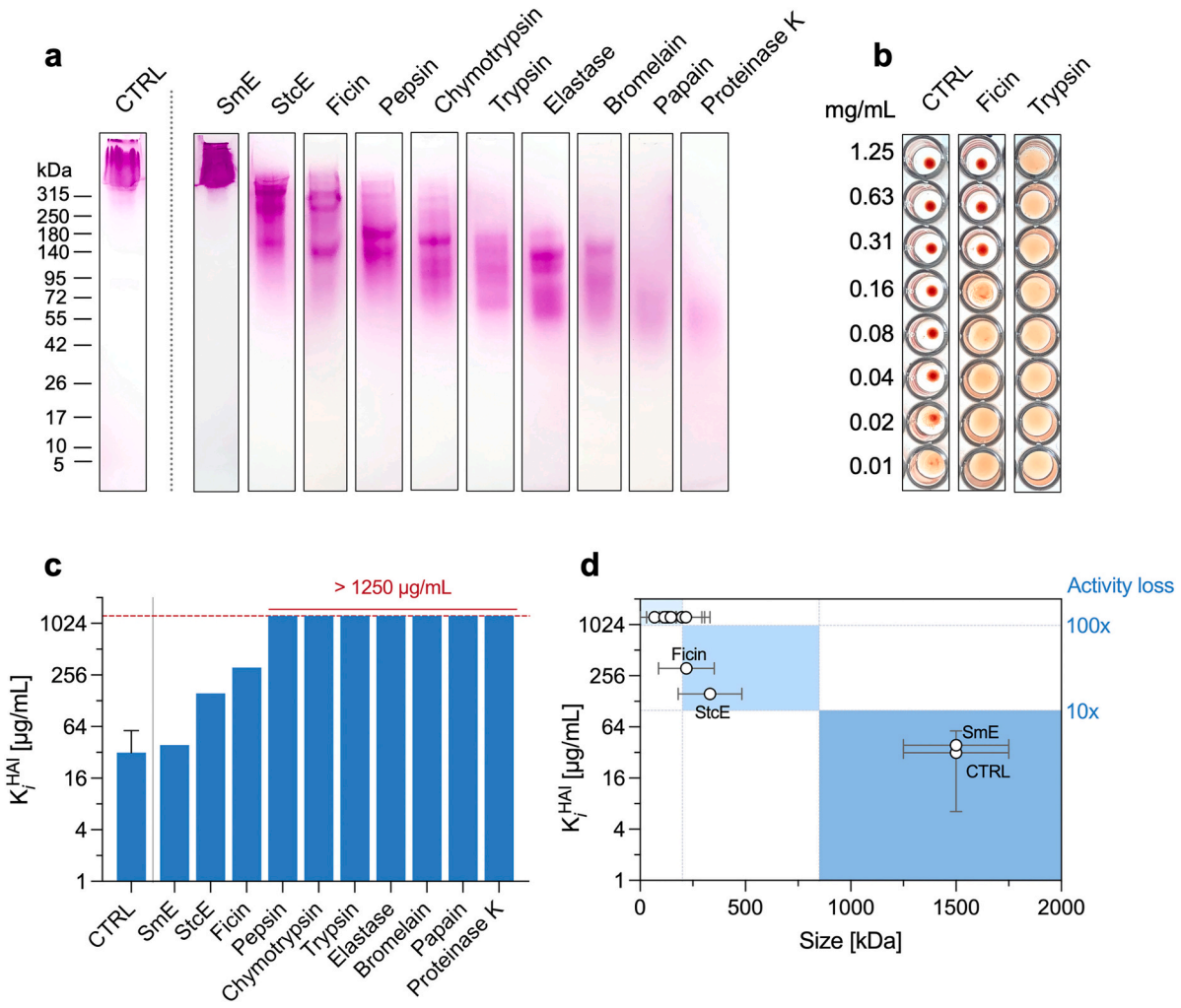

Fig. 4. Quantifying the effect of the size of mucins on the inhibition activity on virus induced hemagglutination. Bovine submaxillary mucin (BSM) was digested with specific and unspecific proteases to obtain mucin fragments of different sizes. (a) Cleavage effectiveness was assessed by SDS-PAGE and PAS staining. (b) The antiviral activity of the fragmented BSM was assessed by hemagglutination inhibition assay (reported only the control sample (PBS), ficin, and trypsin as representative of active, partially, and inactive samples, respectively). (c) Inhibition constant (K_i^{HAI}) defined as the lowest concentration of BSM or BSM fragments that is able to inhibit agglutination. Results are displayed as the average (± SD, for some samples not visible as being too small) of $N = 3$ (except $N_{CTRL} = 15$) measurements. No antiviral effect is observed for digests obtained using pepsin, chymotrypsin, trypsin, elastase, bromelain, papain, and proteinase K therefore the K_i^{HAI} is set at the maximum concentration tested (*i.e.*, 1250 µg/mL) (d) Relationship between K_i^{HAI} and the size of mucin or mucin fragments with activity regions highlighted in blue. Arbitrary thresholds at about 850 and 200 kDa have been set to delineate regions where the activity undergoes reduction by one and two orders of magnitude.

3.2. Glycan contribution to mucin's antiviral activity against influenza

To investigate the structural determinants for influenza virus binding to mucins, mucin glycans from BSM were subjected to enzymatic or chemical removal of monosaccharides or specific glycans (Table 1, Fig. 3a). Here, sialic acid was cleaved from purified BSM using a commercial mixture of sialidases (SialEXO®) with broad activity for α2–6, α2–3, and α2–8-linked sialic acids on both *O*- and *N*-glycans. Removal of *N*-glycans was achieved with PNGase-F, which is an amidase cleaving between the innermost GlcNAc and asparagine residues of almost all *N*-linked oligosaccharides. Since no universal enzyme for complete *O*-glycan removal from the heavily *O*-glycosylated regions of mucins has been identified so far, we chemically removed unsubstituted C3 GalNAc residues unspecifically by oxidative *β*-elimination following a protocol with minimal or no peptide core cleavage (Fig. S3) [32].

Product formation after glycan removal was analyzed using specific lectins for defined carbohydrates (Fig. 3b). After comparing the binding of wheat germ agglutinin (WGA), *Sambucus nigra* lectin (SNA), and Maakia amurensis lectin II (MAL-II) to BSM, we used fluorescently labeled WGA to follow the efficiency of sialic acid removal on BSM as it showed the highest binding and best reproducibility [48] (Fig. S4). To visualize *N*-linked glycans, we used fluorescently labeled high-mannose-binding concanavalin A (Con-A), as Con-A specifically binds to *N*-glycans due to their high mannose content [49,50]. Periodic acid-Schiff stain was used as a universal method to visualize the glycans following the unspecific release of mucin glycans through *β*-elimination treatment [51]. The SDS-PAGE showed that PNGase-F treatment effectively removed *N*-glycans, while *β*-elimination led to the removal of nearly all glycans. In contrast, WGA staining of sialic acid revealed a reduced but still present sialylated sugars even after treatment with sialidases. Additionally, a consistent proportion of sialic acids in BSM has been reported to be acetylated [52]. This, along with residue inaccessibility, may explain the partial resistance of sialic acids to enzymatic cleavage [53]. Further, quantitative sialic acid measurements (NANA assay) showed that the sialidases cleaved approximately 67 % (Fig. S5) of the total sialic acid on BSM, in agreement with previous findings.

Next, the potential of BSM or deglycosylated derivatives of BSM to prevent binding of seasonal influenza virus (A/Panama/2007/99 (H3N2)) to human red blood cells (hRBC) was investigated by the well-established HAI assay (Fig. 3d). The inhibition effectiveness was

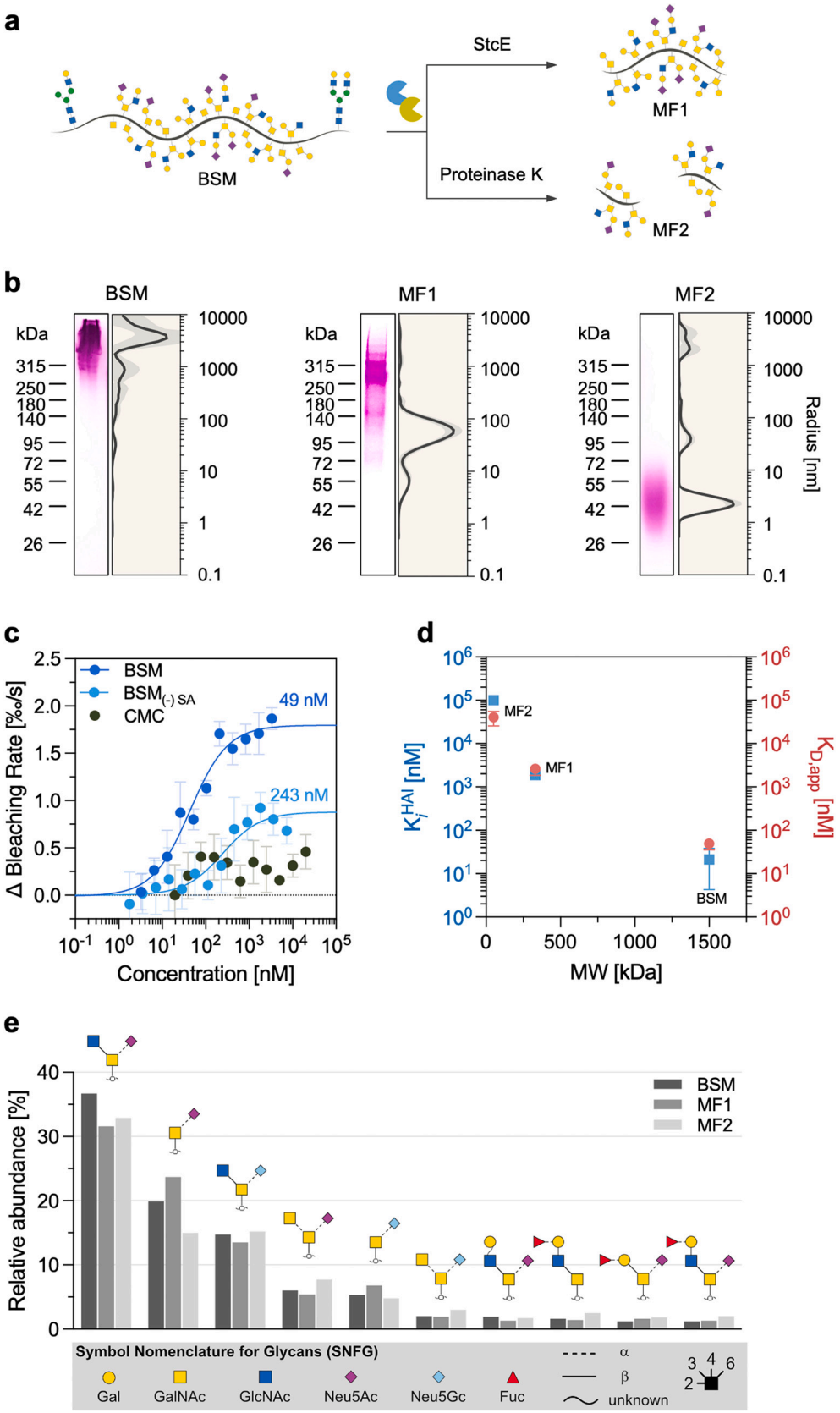

(caption on next page)

Fig. 5. Mucin fragments have virus-binding and antiviral capacity in a size-dependent manner. (a) Illustration of the digestion of mucin from the bovine submaxillary gland (BSM) with StcE (MF1) or proteinase K (MF2). (b) SDS-PAGE/PAS staining and dynamic light scattering of the native BSM, and the purified mucin fragments. (c) Microscale thermophoresis (MST) change in the bleaching rate upon binding of BSM at different concentrations to fluorescently labeled R18 A/X31 virus at the steady state. Desialylated BSM ($BSM_{(-)SA}$) and carboxymethyl cellulose (CMC) served as controls. Binding constants are described as apparent dissociation constants ($K_{D,app}$). Each data point represents the average values of $N = 4$ experiments and the error bars show the standard deviation. Data points were fitted according to the mass-action law function to calculate $K_{D,app}$ values. (d) HAI assay against four hemagglutination units (HAU) A/X31 and the $K_{D,app}$ measured by MST. (e) Relative abundance and putative structures of the top-10 *O*-glycans in BSM, MF1, and MF2.

expressed as K_i^{HAI} representing the lowest concentration of inhibitor that successfully inhibits hemagglutination at four hemagglutination units (4 HAU). BSM was used as a control, showing the highest inhibition constant (K_i^{HAI}) of about 30 μg/mL (21.3 nM) (Fig. 3e). Interestingly, even though the purification of BSM increased its overall quality by enriching the mucin content and lowering the contaminants, this was not translated also in a variation of its antiviral activity as measured by the HAI assay (Fig. S6). This observation suggests that protein contaminants which are present in BSM do not, or minimally interfere with the binding of mucins to the virus.

We found that partially removing sialic acids from BSM significantly decreases by over 10-fold but does not eliminate antiviral inhibitory activity (K_i^{HAI} = 380 μg/mL). Since sialic acids was not completely cleaved by sialidase treatment, this might explain the observed remnant activity. We did not individually evaluate the contributions of the two types of sialic acid (Neu5Ac, Neu5Gc) to the antiviral efficacy of BSM. However, previous studies on IAV/H3N2 showed significantly reduced infectivity in Neu5Gc-rich cells compared to Neu5Ac, but no differences in membrane fusion kinetics [54]. Given the Neu5Ac predominance in BSM (>65 %), it is reasonable to assume that the observed antiviral activity is primarily driven by Neu5Ac.

Removal of *N*-glycans does not significantly affect the antiviral activity of BSM. This observation could be related to different factors; firstly, *N*-linked glycans are comparatively less abundant than *O*-linked glycans. Glycosylation predictions using NetNGlyc [55] indicate that <1 % of the asparagine residues as part of the N-X-S/T sequon in the MUC19 sequence are glycosylated; in contrast, predictions from NetOGlyc [56] reveals that approximately 24 % of serine and threonine residues are *O*-glycosylated (Fig. 3c). Secondly, the glycomic analysis highlighted that the analyzed *N*-glycans from BSM are low in sialic acids, which we confirmed to be pivotal for influenza inhibition. The low abundancy and scarce sialylation might explain the negligible participation of *N*-glycans in virus interaction. Previous studies proposed *N*-glycosylation as key feature in mucin synthesis, stability, and folding rather than direct interaction with viruses [57]. Although the *N*-glycans of mucin might have a negligible effect on the antiviral activity of isolated mucin, it is important to note that mucus consists also of other non-mucin proteins (*e.g.*, lysozyme, lactoferrin, surfactant proteins). Other *N*-glycosylated non-mucin proteins may interact with the virus in ways that are underestimated in isolated BSM.

On the other hand, removing all glycans unspecifically, resulted in abolished antiviral inhibitory activity, with no inhibition observed even at the highest concentration tested ($K_i^{HAI} > 1250$ μg/mL), suggesting a predominant role of mucin *O*-glycans in influenza virus engagement. It is worth mentioning that because of the unspecificity of the *β*-elimination reaction, removal of *O*-glycans implies the simultaneous removal of sialic acid, accounting then for the combined effect of *O*-glycans and sialic acid. Nevertheless, these findings point at sialylated *O*-glycans as the primary interaction sites for influenza virus, while exclude *N*-glycans from playing a significant role in viral binding. This aligns with previous findings that influenza virus HA interacts not only with the terminal sialic acids but also with the underlying monosaccharide components (*e.g.*, LacNAc repeats, [58]) of sialoglycans and, to a lesser extent with non-sialylated glycans [59].

3.3. Mucin size correlates with antiviral effect

The size of polymeric antiviral materials can impact its efficacy in binding to the virus [60,61], therefore, we investigated how the size of the mucin polymers influences its antiviral effect. Because of their polymeric structure and high glycosylation, mucins exhibit intrinsic resistance to proteolytic degradation. Complete degradation requires an arsenal of carbohydrate-active enzymes and proteases able to degrade the glycans and the peptide core [62]. To obtain mucin glycosylated fragments of different sizes, we digested BSM using proteases with different cleavage specificities (Table S1). We selected a diverse set of proteolytic enzymes, including animal and plant proteases as well as mucinases, and conducted the reactions under optimal conditions specific to each enzyme's activity. After overnight digestion, cleavage efficiency was assessed by SDS-PAGE and PAS staining, while the antiviral activity of the fragmented BSM was measured by hemagglutination inhibition.

Intact purified BSM becomes visible by PAS after agarose gel electrophoresis as a broad band in the MDa range, with an estimated apparent molecular weight of about 1.5 MDa (Fig. S1b) [63]. Except for *Serratia marcescens* Enhancin (SmE), the digestion of BSM with all the proteases displayed a mass distribution of the fragments at lower molecular mass range compared to the intact BSM (Fig. 4a). Among the tested proteases, proteinase K demonstrated the highest efficiency in degrading mucin, producing glycosylated fragments ranging from approximately 40 to 70 kDa. Fragments in such a size range could be indicative of the smallest structural tandem repeat units that retain extensive glycosylation and are resistant to proteolytic cleavage. Antiviral activity assessed by hemagglutination inhibition was observed only for the BSM digests obtained with SmE, StcE, and ficin at a concentration up to 1250 μg/mL (Fig. 4b, c). In contrast, digests from all the other enzymes, including pepsin, chymotrypsin, trypsin, elastase, bromelain, papain, and proteinase K, exhibited no visible antiviral activity (*i.e.*, K_i^{HAI} values exceeding 1250 μg/mL) (Fig. 4c). Based on the mass distribution of the BSM fragments observed on the SDS-PAGE gel, a discernible size-activity relationship can be inferred. Specifically, a trend emerges indicating that the antiviral activity of the glycosylated fragments is dependent on their size (Fig. 4d), specifically as the molecular weight increases, the K_i^{HAI} decreases in a non-linear manner, suggesting that larger structures exhibit higher antiviral activity. Notably, rough thresholds can be traced around 850 and 200 kDa defining regions where the size-dependent activity drops by a factor of 10× and 100×.

3.4. Glycosylated mucin fragments retain the virus-binding capacity and antiviral properties in a size-dependent manner

The hemagglutination inhibition assay of BSM digests indicates that the size of the mucin fragments (MFs) influences their antiviral efficacy. To explore this relationship further, we investigated how the molecular size of these fragments impacts their binding affinity to the influenza virus. We enriched and purified glycosylated MFs with varying molecular weights and different antiviral activities. Among the enzymatically derived mucin fragments, those obtained using StcE (MF1) and proteinase K (MF2) were selected for further analysis as they represented the largest and smallest fragments detectable by SDS-PAGE in our experimental conditions (Fig. 5a). While ficin digestion also generated fragments with distinct antiviral activity, their molecular size and inhibitory potency were comparable to those produced by StcE, making them redundant for further affinity characterization.

Compared to native BSM, which exhibits an apparent molecular weight in the MDa range (Fig. S1b), MF1 and MF2 are revealed by PAS at

~330 kDa and ~ 50 kDa, respectively. Additionally, the hydrodynamic radii of these fragments differ by several order of magnitudes, with intact BSM measuring over 2000 nm, while for MF1 and MF2 measuring 60 nm and 2.5 nm, respectively (Fig. 5b). In terms of sialic acid composition, both fragments have less abundancy compared to BSM. Specifically, BSM contains over 550 mol of SA per mol of protein, while MF1 and MF2 contain approximately 390 and 26 mol of SA per mol of protein, respectively. When normalized by the apparent molecular weight to express the density of SA, MF1 shows the highest density at 1.2 mol/kDa, surpassing both BSM (0.4 mol/kDa) and MF2 (0.5 mol/kDa) (Fig. S7). This suggests that both MFs retain a high sialic acid density. Structurally these fragments could mainly, if not only, be constituted of the highly glycosylated regions (*i.e.*, PTS domains) of mucin, with minimum or any non-glycosylated parts.

The HAI assay revealed that MF1 and MF2 have HAI constants (K_i^{HAI}) of 1.88 μM (0.63 mg/mL) and 100 μM (5 mg/mL), respectively (Fig. S8 a, c). When compared to BSM, these values reflect a reduction of antiviral activity by approximately two and four orders of magnitude for MF1 and MF2, respectively. Previous studies with sialylated bioinspired brush polymers (~400 kDa) demonstrated inhibition of influenza virus (H1N1 subtype) with a K_i^{HAI} of 0.24 μM, placing its activity in a comparable range to MF1 [64].

Next, we characterized the affinity at which the different BSM derivatives bind to influenza A/X31 virus (H3N2 subtype), which is a subtype antigenically similar to A/Panama/2007/99 but with differences in the glycosylation sites [65]. Microscale thermophoresis (MST) experiments showed that the intact BSM had an apparent dissociation constant ($K_{D,app}$) in the nanomolar range (49 nM) (Fig. 5c). Desialylated BSM ($BSM_{(-)SA}$) was used as binding control (*i.e.*, expected lower binding than BSM), while carboxymethyl cellulose (CMC), a high molecular weight natural polymer similar to BSM in viscosity and charge, served as a negative control binder. Partial cleavage of sialic acid (~67 % efficacy, Fig. S5) from BSM reduced its binding affinity for the virus by approximately 5-fold (243 nM). This suggests that while reduced sialylation in BSM still permits virus binding, it does so with reduced effectiveness, as indicated by the lower affinity and binding amplitude compared to intact BSM.

MST measurements with MF1 and MF2 (Fig. S8 b, d) supported the HAI assay findings, showing very good agreement between $K_{D,app}$ and K_i^{HAI} values (Fig. S9). The reduction in fragment size weakened both the binding avidity and the antiviral inhibitory capacity, evidenced by an exponential increase in both $K_{D,app}$ and K_i^{HAI} (Fig. 5d). These observations are consistent with the notion that larger glycoprotein structures can present multiple binding sites, thereby enhancing overall viral binding and inhibitory activity [60,64,66,67]. The ability of the MFs to bind to the virus suggests that the glycan structures involved in virus attachment are still present in the small fragments. *O*-glycan analysis showed that the same glycans identified in intact BSM are still present, and with comparable relative abundance, on MF1 and MF2 (Fig. 5e). Interestingly, assuming the MFs as individual (MF2) or serial repetition (MF1) of tandem repeats of the highly glycosylated regions (PTS) of MUC19, we can conclude that the glycosylation pattern is conserved and homogeneously distributed on the tandem repeats of mucin. Yet, the reduced size and reduced multiplicity of binding sites results in weaker and less effective inhibition. Previous studies have proposed that an ideal antiviral polymer should position sialic acid residues at intervals around the intra-hemagglutinin spacing (~4.5 nm) while maintaining an overall polymer length larger than the inter-hemagglutinin trimer spacing (~14 nm) [64,68]. This configuration would ensure a high local concentration of sialic acids and the ability to bridge multiple hemagglutinin trimers, thereby enhancing multivalent binding and viral inhibition. Based on these criteria, MF2 (~2.5 nm radius) alone as an antiviral could roughly span the intra-hemagglutinin distance giving place to bivalent binding, but it fails to meet the necessary spatial arrangement for inter-hemagglutinin binding, limiting its capacity for effective viral engagement. Similarly, although MF1 could potentially meet both criteria due to its larger size (~60 nm radius) and high SA abundance, its antiviral activity may still be insufficient on its own. However, rather than functioning independently, mucin fragments could serve as versatile building blocks for larger antiviral architectures (*e.g.*, linear polymers, polymeric networks), leveraging both their glycan diversity and steric effects.

4. Discussion

The role of glycans of mucins on the interaction with the influenza spike proteins hemagglutinin and neuraminidase is still under debate and is most probably strain dependent. How this intertwines with polymer size adds an additional layer of complexity. Our findings highlight the crucial role of sialylated *O*-glycans in defining the antiviral activity of BSM, whereas *N*-glycans contribute minimally, likely due to their low abundance and paucity of sialylation. While partial removal of sialic acid reduced but did not completely abolish antiviral activity, full glycan removal eliminated inhibition altogether, underscoring the importance of *O*-glycans.

Our results suggest that rather than only the terminal sialic acid residues, the entire structure of sialylated *O*-glycans is critical for hemagglutinin (HA) binding and viral inhibition. This observation aligns with prior evidence suggesting that influenza HA does not simply recognize terminal sialic acids but rather engages also with the inner monosaccharides of the sialoglycan.

We also demonstrated a strong size-dependent effect on antiviral efficacy. Mucin fragments of different size, displaying the same *O*-glycosylation pattern as full-length mucin, were produced by proteolytic digestion. Intact BSM (MDa scale) exhibited high viral binding affinity in the nanomolar range and potent inhibition, whereas smaller mucin fragments (MF1, ~330 kDa, and MF2, ~50 kDa) showed drastically reduced antiviral activity, with K_i^{HAI} values of 0.63 mg/mL and 5 mg/mL, respectively. Binding affinity decreased similarly, with $K_{D,app}$ values increasing to 2.6 μM for MF1 and 40 μM for MF2. The non-linear decrease in antiviral activity upon fragmentation suggest that molecular size, beyond glycan composition alone, plays a dominant role in optimizing multivalent binding and inhibition. Furthermore, when comparing the effects of size modulation (*i.e.*, BSM *vs* MFs) with glycan density modulation (*i.e.*, BSM *vs* desialylated BSM), we clearly observe a reduction in both inhibition and binding affinity that is more dramatic with size reduction than with glycan density changes. While affinity contributes to viral capture, the extended polymer network of full-length mucins likely enhances avidity and sterically excludes viral particles from host receptors. However, our study focused solely on the H3N2 subtype of influenza A virus, and given the structural diversity of haemagglutinin (HA) across different IAV subtypes, further investigations are needed to determine whether these findings extend in a similar fashion to other influenza strains.

Additionally, the ability of small mucin fragments, such as MF2 to bind influenza virus, points to potential applications as viral decoys for biopolymers or nanoparticles for targeted drug delivery. Importantly, these mucin-derived fragments, as natural glycopeptides, present minimal functional virus-binding units with naturally evolved glycan diversity and optimized spatial distribution. Unlike biomimetic polymers, which require meticulous design to mimic these features and may pose biodegradability challenges, mucin-derived glycopeptides offer a natural alternative. They inherently combine functional efficacy from evolved glycan architectures with high biocompatibility, potentially at a lower cost. This dual advantage positions them as promising candidates for the development of novel broad-spectrum antiviral biomaterials, where the combination of steric contribution and multiple weak binding interactions can significantly amplify inhibitory effects. Further engineering of hydrogels or nanoparticles harboring such building blocks can lead to novel antiviral materials with economic use of antiviral ligands arranged in nanoclusters.

In conclusion, our findings on the structural determinants of mucins

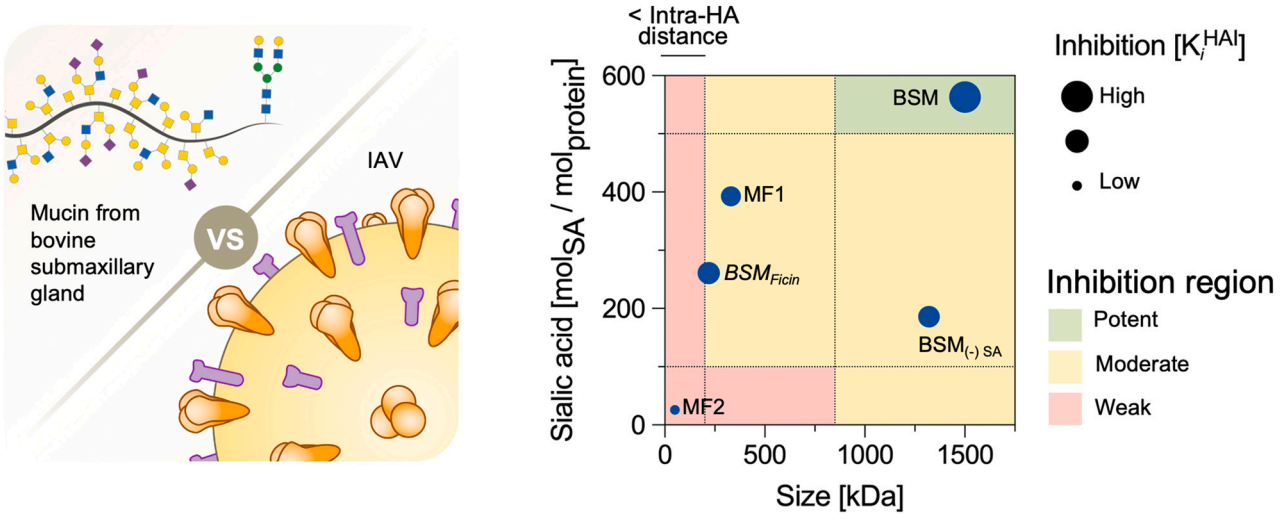

Fig. 6. Summary of the impact of the size and sialic acids of mucin BSM on IAV inhibition, according to the findings herein reported. The multiple variable plot represent the chemical space defined by the size of BSM and BSM fragments and their sialic acid abundancy. An additional layer is provided by the inhibition activity expressed as K_i^{HAI}. Activity regions are defined and colour coded according to arbitrary thresholds for size (200, 850 kDa, see Fig. 4d) and sialic acid abundancy (100, 500 $mol_{SA}/mol_{protein}$). The SA abundance for BSM_{Ficin} was extrapolated given the size similarity to MF1.

offer broad guidelines for designing synthetic polymers with mucin-mimetic antiviral activity (Fig. 6). Our data suggest that molecular size should be prioritized over sialoglycan density. Specifically, linear polymers in the megadalton (MDa) range (>850 kDa) bearing sialylated glycans are expected to achieve viral inhibition comparable to bovine submaxillary mucin (BSM). Simple *O*-glycans should be favored over more complex and synthetically demanding *N*-glycans. Beyond simple presenting sialic acids, the architecture of *O*-glycans plays a direct role in modulating viral interactions. However, for optimal antiviral effects, specific *O*-glycan structures should be individually investigated and systematically compared.

CRediT authorship contribution statement

Cosmin Butnarasu: Writing – original draft, Visualization, Investigation, Formal analysis, Conceptualization. **Marc Safferthal:** Writing – review & editing, Visualization, Methodology, Formal analysis. **Jolly Thomas:** Writing – review & editing, Methodology, Formal analysis. **Tatyana L. Povolotsky:** Writing – review & editing, Resources. **Robyn Diehn:** Writing – review & editing, Resources. **Kerstin Fentker:** Writing – review & editing, Visualization, Methodology, Investigation, Formal analysis. **Philipp Mertins:** Writing – review & editing, Supervision, Resources, Funding acquisition, Formal analysis. **Kevin Pagel:** Writing – review & editing, Resources, Funding acquisition. **Daniel C. Lauster:** Writing – review & editing, Writing – original draft, Supervision, Resources, Project administration, Funding acquisition, Formal analysis, Conceptualization.

Declaration of competing interest

The authors declare that they have no known competing financial interests or personal relationships that could have appeared to influence the work reported in this paper.

Acknowledgements

We are grateful to Stacy Malaker for providing us with pet28a_SmE that we used to express SmE, Junqioa Jia in the Markus Wahl lab (Freie Universität Berlin) for support in expression and purification of StcE, and professor Dr. Joachim Heberle for giving us access to his Monolith instrument to perform MST studies. The project was realized with research infrastructure and support provided by the Research Building SupraFAB realized with funds from the Federal Government (BMBF) and the State of Berlin. DCL is grateful for financial support from the federal ministry of education and research (BMBF) funded project MucPep (FKZ: 13XP511). The authors acknowledge the financial support of the Collaborative Research Center "Dynamic Hydrogels at Biological Interfaces" (CRC 1449) funded by the Deutsche Forschungsgemeinschaft (DFG, German Research Foundation) – Project ID 431232613– SFB 1449 (sub-projects C03, Z01 and the IRTG).

Appendix A. Supplementary data

Supplementary data to this article can be found online at https://doi.org/10.1016/j.ijbiomac.2025.142357.

Data availability

Data will be made available on request.

References

[1] L. Mackenzie, World Health Organization - The burden of Influenza. https://www.who.int/news-room/feature-stories/detail/the-burden-of-influenza#:~:text=Diseaseburdenfromseasonalinfluenza&text=Influenza%2Cortheflu%2Cis,viruses%2Cafterthecommoncold, 2024.
[2] S. Malik, M. Asghar, Y. Waheed, Outlining recent updates on influenza therapeutics and vaccines: a comprehensive review, Vaccine X. 17 (2024) 100452, https://doi.org/10.1016/j.jvacx.2024.100452.
[3] L. Jiang, H. Chen, C. Li, Advances in deciphering the interactions between viral proteins of influenza a virus and host cellular proteins, Cell Insight 2 (2023) 100079, https://doi.org/10.1016/j.cellin.2023.100079.
[4] C.L. Wardzala, A.M. Wood, D.M. Belnap, J.R. Kramer, Mucins inhibit coronavirus infection in a glycan-dependent manner, ACS Cent. Sci. 8 (2022) 351–360, https://doi.org/10.1021/acscentsci.1c01369.
[5] I. Ethan, G. Kira, S. Daniel, G.T. B, H. Kajal, K. Mehmet, S. Sanju, P. Melissa, D.G. A., S.M. A, Membrane-Tethered Mucin 1 Is Stimulated by Interferon and Virus Infection in Multiple Cell Types and Inhibits Influenza A Virus Infection in Human Airway Epithelium, MBio 13 (2022), https://doi.org/10.1128/mbio.01055-22 e01055–22.
[6] M. Kretschmer, R. Ceña-Diez, C. Butnarasu, V. Silveira, I. Dobryden, S. Visentin, P. Berglund, A. Sönnerborg, O. Lieleg, T. Crouzier, H. Yan, Synthetic mucin gels with self-healing properties augment lubricity and inhibit HIV-1 and HSV-2 transmission, Adv. Sci. 9 (2022) 2203898, https://doi.org/10.1002/advs.202203898.
[7] R. Bansil, B.S. Turner, Mucin structure, aggregation, physiological functions and biomedical applications, Curr. Opin. Colloid Interface Sci. 11 (2006) 164–170, https://doi.org/10.1016/j.cocis.2005.11.001.

[8] M. Cohen, X.-Q. Zhang, H.P. Senaati, H.-W. Chen, N.M. Varki, R.T. Schooley, P. Gagneux, Influenza a penetrates host mucus by cleaving sialic acids with neuraminidase, Virol. J. 10 (2013) 321, https://doi.org/10.1186/1743-422X-10-321.
[9] J.N.S.S. Couceiro, J.C. Paulson, L.G. Baum, Influenza virus strains selectively recognize sialyloligosaccharides on human respiratory epithelium; the role of the host cell in selection of hemagglutinin receptor specificity, Virus Res. 29 (1993) 155–165, https://doi.org/10.1016/0168-1702(93)90056-S.
[10] J. Mayr, K. Lau, J.C.C. Lai, I.A. Gagarinov, Y. Shi, S. McAtamney, R.W.Y. Chan, J. Nicholls, M. von Itzstein, T. Haselhorst, Unravelling the role of O-glycans in influenza a virus infection, Sci. Rep. 8 (2018) 16382, https://doi.org/10.1038/s41598-018-34175-3.
[11] C.M. Spruit, N. Nemanichvili, M. Okamatsu, H. Takematsu, G.-J. Boons, R.P. de Vries, N-Glycolylneuraminic acid in animal models for human influenza a virus, Viruses 13 (2021), https://doi.org/10.3390/v13050815.
[12] T. Takahashi, M. Takano, Y. Kurebayashi, M. Masuda, S. Kawagishi, M. Takaguchi, T. Yamanaka, A. Minami, T. Otsubo, K. Ikeda, T. Suzuki, *N*-Glycolylneuraminic acid on human epithelial cells prevents entry of influenza A viruses that possess *N*-Glycolylneuraminic acid binding ability, J. Virol. 88 (2014) 8445–8456, ee, https://doi.org/10.1128/jvi.00716-14.
[13] L. Kaler, E. Iverson, S. Bader, D. Song, M.A. Scull, G.A. Duncan, Influenza A virus diffusion through mucus gel networks, Commun. Biol. 5 (2022) 249, https://doi.org/10.1038/s42003-022-03204-3.
[14] K. Barnard, B. Alford-Lawrence, D. Buchholz, B. Wasik, J. LaClair, Y. Hai, H. Rebekah, R. Stefan, P. Petar, E. Daugherity, C. Xi, S. Schultz-Cherry, H. Aguilar, V. Ajit, C. Parrish, Modified sialic acids on mucus and erythrocytes inhibit influenza A virus hemagglutinin and neuraminidase functions, J. Virol. 94 (2020) https://doi.org/10.1128/jvi.01567-19. doi:https://doi.org/10.1128/jvi.01567-19.
[15] G. Petrou, T. Crouzier, Mucins as multifunctional building blocks of biomaterials, Biomater. Sci. 6 (2018) 2282–2297, https://doi.org/10.1039/C8BM00471D.
[16] G.W. Hughes, C. Ridley, R. Collins, A. Roseman, R. Ford, D.J. Thornton, The MUC5B mucin polymer is dominated by repeating structural motifs and its topology is regulated by calcium and pH, Sci. Rep. 9 (2019) 17350, https://doi.org/10.1038/s41598-019-53768-0.
[17] R.W.H. Ruigrok, L.J. Calder, S.A. Wharton, Electron microscopy of the influenza virus submembranal structure, Virology 173 (1989) 311–316, https://doi.org/10.1016/0042-6822(89)90248-1.
[18] S. Bhatia, D. Lauster, M. Bardua, K. Ludwig, S. Angioletti-Uberti, N. Popp, U. Hoffmann, F. Paulus, M. Budt, M. Stadtmüller, T. Wolff, A. Hamann, C. Böttcher, A. Herrmann, R. Haag, Linear polysialoside outperforms dendritic analogs for inhibition of influenza virus infection in vitro and in vivo, Biomaterials 138 (2017) 22–34, https://doi.org/10.1016/j.biomaterials.2017.05.028.
[19] C.S. Delaveris, E.R. Webster, S.M. Banik, S.G. Boxer, C.R. Bertozzi, Membrane-tethered mucin-like polypeptides sterically inhibit binding and slow fusion kinetics of influenza A virus, Proc. Natl. Acad. Sci. 117 (2020) 12643–12650, https://doi.org/10.1073/pnas.1921962117.
[20] W.J. Lees, A. Spaltenstein, J.E. Kingery-Wood, G.M. Whitesides, Polyacrylamides Bearing Pendant .alpha.-Sialoside Groups Strongly Inhibit Agglutination of Erythrocytes by Influenza A Virus: Multivalency and Steric Stabilization of Particulate Biological Systems, J. Med. Chem. 37 (1994) 3419–3433, https://doi.org/10.1021/jm00046a027.
[21] S.-K. Choi, M. Mammen, G.M. Whitesides, Generation and in situ evaluation of libraries of poly(acrylic acid) presenting Sialosides as side chains as polyvalent inhibitors of influenza-mediated Hemagglutination, J. Am. Chem. Soc. 119 (1997) 4103–4111, https://doi.org/10.1021/ja963519x.
[22] V.R. Kohout, C.L. Wardzala, J.R. Kramer, Synthesis and biomedical applications of mucin mimic materials, Adv. Drug Deliv. Rev. 191 (2022) 114540, https://doi.org/10.1016/j.addr.2022.114540.
[23] T. Jaroentomeechai, R. Karlsson, F. Goerdeler, F.K.Y. Teoh, M.N. Grønset, D. de Wit, Y.-H. Chen, S. Furukawa, V. Psomiadou, R. Hurtado-Guerrero, E.E. Vidal-Calvo, A. Salanti, T.J. Boltje, L.J. van den Bos, C. Wunder, L. Johannes, K. T. Schjoldager, H.J. Joshi, R.L. Miller, H. Clausen, S.Y. Vakhrushev, Y. Narimatsu, Mammalian cell-based production of glycans, glycopeptides and glycomodules, Nat. Commun. 15 (2024) 9668, https://doi.org/10.1038/s41467-024-53738-9.
[24] M. Safferthal, L. Bechtella, A. Zappe, G.M. Vos, K. Pagel, Labeling of mucin-type O-Glycans for quantification using liquid chromatography and fluorescence detection, ACS Meas. Sci. Au. 4 (2024) 223–230, https://doi.org/10.1021/acsmeasuresciau.3c00071.
[25] J. Kim, C. Ryu, J. Ha, J. Lee, D. Kim, M. Ji, C.S. Park, J. Lee, D.K. Kim, H.H. Kim, Structural and quantitative characterization of mucin-type O-Glycans and the identification of O-glycosylation sites in bovine submaxillary mucin, Biomolecules 10 (2020), https://doi.org/10.3390/biom10040636.
[26] V.J. Schömig, B.T. Käsdorf, C. Scholz, K. Bidmon, O. Lieleg, S. Berensmeier, An optimized purification process for porcine gastric mucin with preservation of its native functional properties, RSC Adv. 6 (2016) 44932–44943, https://doi.org/10.1039/C6RA07424C.
[27] H. Rulff, R.F. Schmidt, L.-F. Wei, K. Fentker, Y. Kerkhoff, P. Mertins, M.A. Mall, D. Lauster, M. Gradzielski, Comprehensive characterization of the viscoelastic properties of bovine submaxillary mucin (BSM) hydrogels and the effect of additives, Biomacromolecules (2024), https://doi.org/10.1021/acs.biomac.4c00153.
[28] C.S. Hughes, S. Foehr, D.A. Garfield, E.E. Furlong, L.M. Steinmetz, J. Krijgsveld, Ultrasensitive proteome analysis using paramagnetic bead technology, Mol. Syst. Biol. 10 (2014) 757, https://doi.org/10.15252/msb.20145625.
[29] J. Rappsilber, Y. Ishihama, M. Mann, Stop and go extraction tips for matrix-assisted laser desorption/ionization, nanoelectrospray, and LC/MS sample pretreatment in proteomics, Anal. Chem. 75 (2003) 663–670, https://doi.org/10.1021/ac026117i.
[30] S. Tyanova, T. Temu, J. Cox, The MaxQuant computational platform for mass spectrometry-based shotgun proteomics, Nat. Protoc. 11 (2016) 2301–2319, https://doi.org/10.1038/nprot.2016.136.
[31] M.E. Ritchie, B. Phipson, D. Wu, Y. Hu, C.W. Law, W. Shi, G.K. Smyth, Limma powers differential expression analyses for RNA-sequencing and microarray studies, Nucleic Acids Res. 43 (2015) e47, https://doi.org/10.1093/nar/gkv007.
[32] T.A. Gerken, R. Gupta, N. Jentoft, A novel approach for chemically deglycosylating O-linked glycoproteins. The deglycosylation of submaxillary and respiratory mucins, Biochemistry 31 (1992) 639–648, https://doi.org/10.1021/bi00118a002.
[33] P.H. Jensen, N.G. Karlsson, D. Kolarich, N.H. Packer, Structural analysis of N- and O-glycans released from glycoproteins, Nat. Protoc. 7 (2012) 1299–1310, https://doi.org/10.1038/nprot.2012.063.
[34] R. Schmid, S. Heuckeroth, A. Korf, A. Smirnov, O. Myers, T.S. Dyrlund, R. Bushuiev, K.J. Murray, N. Hoffmann, M. Lu, A. Sarvepalli, Z. Zhang, M. Fleischauer, K. Dührkop, M. Wesner, S.J. Hoogstra, E. Rudt, O. Mokshyna, C. Brungs, K. Ponomarov, L. Mutabdžija, T. Damiani, C.J. Pudney, M. Earll, P. O. Helmer, T.R. Fallon, T. Schulze, A. Rivas-Ubach, A. Bilbao, H. Richter, L.-F. Nothias, M. Wang, M. Orešič, J.-K. Weng, S. Böcker, A. Jeibmann, H. Hayen, U. Karst, P.C. Dorrestein, D. Petras, X. Du, T. Pluskal, Integrative analysis of multimodal mass spectrometry data in MZmine 3, Nat. Biotechnol. 41 (2023) 447–449, https://doi.org/10.1038/s41587-023-01690-2.
[35] A.V. Everest-Dass, J.L. Abrahams, D. Kolarich, N.H. Packer, M.P. Campbell, Structural feature ions for distinguishing N- and O-linked glycan isomers by LC-ESI-IT MS/MS, J. Am. Soc. Mass Spectrom. 24 (2013) 895–906, https://doi.org/10.1007/s13361-013-0610-4.
[36] M. Grabarics, M. Lettow, C. Kirschbaum, K. Greis, C. Manz, K. Pagel, Mass spectrometry-based techniques to elucidate the sugar code, Chem. Rev. 122 (2022) 7840–7908, https://doi.org/10.1021/acs.chemrev.1c00380.
[37] A. Ceroni, K. Maass, H. Geyer, R. Geyer, A. Dell, S.M. Haslam, GlycoWorkbench: a tool for the computer-assisted annotation of mass spectra of glycans, J. Proteome Res. 7 (2008) 1650–1659, https://doi.org/10.1021/pr7008252.
[38] M.A. Rosenfeld, F.L. Kearns, J. Chongsaritsinsuk, A. Steigmeyer, K.E. Mahoney, T. M. Lucas, D. Ince, A. Battison, M.A. Hollenhorst, D.J. Shon, C.R. Bertozzi, M. J. Farracane, M.A. Lemmon, S.A. Malaker, R.E. Amaro, Glycoproteomic landscape and structural dynamics of TIM family immune checkpoints enabled by mucinase SME and molecular dynamics simulations, Biophys. J. 123 (2024) 14a, https://doi.org/10.1016/j.bpj.2023.11.205.
[39] K. Jiang, H. Yan, C. Rickert, M. Marczynski, K. Sixtensson, F. Vilaplana, O. Lieleg, T. Crouzier, Modulating the bioactivity of mucin hydrogels with crosslinking architecture, Adv. Funct. Mater. 31 (2021) 2008428, https://doi.org/10.1002/adfm.202008428.
[40] K.A. Ramsey, Z.L. Rushton, C. Ehre, Mucin agarose gel electrophoresis: Western blotting for high-molecular-weight glycoproteins, J. Vis. Exp. (2016), https://doi.org/10.3791/54153.
[41] D.J. Thornton, J.K. Sheehan, I. Carlstedt, in: J.M. Walker (Ed.), Identification of Glycoproteins on Nitrocellulose Membranes and Gels BT - Basic Protein and Peptide Protocols, Humana Press, Totowa, NJ, 1994, pp. 119–128, https://doi.org/10.1385/0-89603-268-X:119.
[42] J.A.C. Stein, A. Ianeselli, D. Braun, Kinetic microscale thermophoresis for simultaneous measurement of binding affinity and kinetics, Angew. Chemie Int. Ed. 60 (2021) 13988–13995, https://doi.org/10.1002/anie.202101261.
[43] G. Tettamanti, W. Pigman, Purification and characterization of bovine and ovine submaxillary mucins, Arch. Biochem. Biophys. 124 (1968) 41–50, https://doi.org/10.1016/0003-9861(68)90301-9.
[44] M. Marczynski, C. Kimna, O. Lieleg, Purified mucins in drug delivery research, Adv. Drug Deliv. Rev. 178 (2021) 113845, https://doi.org/10.1016/j.addr.2021.113845.
[45] Y. Chen, Y.H. Zhao, T.B. Kalaslavadi, E. Hamati, K. Nehrke, A.D. Le, D.K. Ann, R. Wu, Genome-wide search and identification of a novel gel-forming mucin MUC19/Muc19 in glandular tissues, Am. J. Respir. Cell Mol. Biol. 30 (2004) 155–165, https://doi.org/10.1165/rcmb.2003-0103OC.
[46] D. Fass, D.J. Thornton, Mucin networks: dynamic structural assemblies controlling mucus function, Curr. Opin. Struct. Biol. 79 (2023) 102524, https://doi.org/10.1016/j.sbi.2022.102524.
[47] J. Kim, J. Lee, Y. Jang, J. Ha, D. Kim, M. Ji, Y.K. Lee, W. Kim, S. You, J. Do, C. Ryu, H.H. Kim, N-glycans of bovine submaxillary mucin contain core-fucosylated and sulfated glycans but not sialylated glycans, Int. J. Biol. Macromol. 138 (2019) 1072–1078, https://doi.org/10.1016/j.ijbiomac.2019.07.108.
[48] V.P. Bhavanandan, A.W. Katlic, The interaction of wheat germ agglutinin with sialoglycoproteins. The role of sialic acid, J. Biol. Chem. 254 (1979) 4000–4008, https://doi.org/10.1016/S0021-9258(18)50686-4.
[49] C.F. Brewer, Interactions of an ovalbumin glycopeptide with concanavalin A, Biochem. Biophys. Res. Commun. 90 (1979) 117–122, https://doi.org/10.1016/0006-291X(79)91597-3.
[50] D. Bojar, L. Meche, G. Meng, W. Eng, D.F. Smith, R.D. Cummings, L.K. Mahal, A useful guide to lectin binding: machine-learning directed annotation of 57 unique lectin specificities, ACS Chem. Biol. 17 (2022) 2993–3012, https://doi.org/10.1021/acschembio.1c00689.
[51] M. Mantle, A. Allen, A colorimetric assay for glycoproteins based on the periodic acid/Schiff stain [proceedings], Biochem. Soc. Trans. 6 (1978) 607–609, https://doi.org/10.1042/bst0060607.
[52] G.M. Vos, K.C. Hooijschuur, Z. Li, J. Fjeldsted, C. Klein, R.P. de Vries, J.S. Toraño, G.-J. Boons, Sialic acid O-acetylation patterns and glycosidic linkage type

determination by ion mobility-mass spectrometry, Nat. Commun. 14 (2023) 6795, https://doi.org/10.1038/s41467-023-42575-x.
[53] H. Yan, M. Hjorth, B. Winkeljann, I. Dobryden, O. Lieleg, T. Crouzier, Glyco-modification of mucin hydrogels to investigate their immune activity, ACS Appl. Mater. Interfaces 12 (2020) 19324–19336, https://doi.org/10.1021/acsami.0c03645.
[54] Y.-A.A. Chien, B.K. Alford, B.R. Wasik, W.S. Weichert, C.R. Parrish, S. Daniel, Single particle analysis of H3N2 influenza entry differentiates the impact of the sialic acids (Neu5Ac and Neu5Gc) on virus binding and membrane fusion, J. Virol. 97 (2023), https://doi.org/10.1128/jvi.01463-22 e01463–22.
[55] R. Gupta, S. Brunak, Prediction of glycosylation across the human proteome and the correlation to protein function, Pac. Symp. Biocomput. (2002) 310–322.
[56] C. Steentoft, S.Y. Vakhrushev, H.J. Joshi, Y. Kong, M.B. Vester-Christensen, K.T. G. Schjoldager, K. Lavrsen, S. Dabelsteen, N.B. Pedersen, L. Marcos-Silva, R. Gupta, E. Paul Bennett, U. Mandel, S. Brunak, H.H. Wandall, S.B. Levery, H. Clausen, Precision mapping of the human O-GalNAc glycoproteome through SimpleCell technology, EMBO J. 32 (2013) 1478–1488, https://doi.org/10.1038/emboj.2013.79.
[57] T. Taniguchi, A.M. Woodward, P. Magnelli, N.M. McColgan, S. Lehoux, S.M. P. Jacobo, J. Mauris, P. Argüeso, N-glycosylation affects the stability and barrier function of the MUC16 mucin, J. Biol. Chem. 292 (2017) 11079–11090, https://doi.org/10.1074/jbc.M116.770123.
[58] A.J. Thompson, N.C. Wu, A. Canales, C. Kikuchi, X. Zhu, B.F. de Toro, F.J. Cañada, C. Worth, S. Wang, R. McBride, W. Peng, C.M. Nycholat, J. Jiménez-Barbero, I. A. Wilson, J.C. Paulson, Evolution of human H3N2 influenza virus receptor specificity has substantially expanded the receptor-binding domain site, Cell Host Microbe 32 (2024) 261–275.e4, https://doi.org/10.1016/j.chom.2024.01.003.
[59] M. Kastner, A. Karner, R. Zhu, Q. Huang, A. Geissner, A. Sadewasser, M. Lesch, X. Wörmann, A. Karlas, P.H. Seeberger, T. Wolff, P. Hinterdorfer, A. Herrmann, C. Sieben, Relevance of host cell surface glycan structure for cell specificity of influenza a viruses, Viruses 15 (2023), https://doi.org/10.3390/v15071507.
[60] M. Wallert, C. Nie, P. Anilkumar, S. Abbina, S. Bhatia, K. Ludwig, J. N. Kizhakkedathu, R. Haag, S. Block, Mucin-inspired, high molecular weight virus binding inhibitors show biphasic binding behavior to influenza A viruses, Small 16 (2020) 2004635, https://doi.org/10.1002/smll.202004635.
[61] J. Vonnemann, S. Liese, C. Kuehne, K. Ludwig, J. Dernedde, C. Böttcher, R.R. Netz, R. Haag, Size dependence of steric shielding and multivalency effects for globular binding inhibitors, J. Am. Chem. Soc. 137 (2015) 2572–2579, https://doi.org/10.1021/ja5114084.
[62] C. Wickström, M.C. Herzberg, D. Beighton, G. Svensäter, Proteolytic degradation of human salivary MUC5B by dental biofilms, Microbiology 155 (2009) 2866–2872, https://doi.org/10.1099/mic.0.030536-0.
[63] L. Shi, K.D. Caldwell, Mucin adsorption to hydrophobic surfaces, J. Colloid Interface Sci. 224 (2000) 372–381, https://doi.org/10.1006/jcis.2000.6724.
[64] S. Tang, W.B. Puryear, B.M. Seifried, X. Dong, J.A. Runstadler, K. Ribbeck, B. D. Olsen, Antiviral agents from multivalent presentation of Sialyl oligosaccharides on brush polymers, ACS Macro Lett. 5 (2016) 413–418, https://doi.org/10.1021/acsmacrolett.5b00917.
[65] M.D. Tate, E.R. Job, Y.-M. Deng, V. Gunalan, S. Maurer-Stroh, P.C. Reading, Playing Hide and Seek: how glycosylation of the influenza virus hemagglutinin can modulate the immune response to infection, Viruses 6 (2014) 1294–1316, https://doi.org/10.3390/v6031294.
[66] G.B. Sigal, M. Mammen, G. Dahmann, G.M. Whitesides, Polyacrylamides bearing pendant α-Sialoside groups strongly inhibit agglutination of erythrocytes by influenza virus: the strong inhibition reflects enhanced binding through cooperative polyvalent interactions, J. Am. Chem. Soc. 118 (1996) 3789–3800, https://doi.org/10.1021/ja953729u.
[67] M. Nagao, Y. Fujiwara, T. Matsubara, Y. Hoshino, T. Sato, Y. Miura, Design of glycopolymers carrying sialyl oligosaccharides for controlling the interaction with the influenza virus, Biomacromolecules 18 (2017) 4385–4392, https://doi.org/10.1021/acs.biomac.7b01426.
[68] V. Bandlow, D. Lauster, K. Ludwig, M. Hilsch, V. Reiter-Scherer, J.P. Rabe, C. Böttcher, A. Herrmann, O. Seitz, Sialyl-LacNAc-PNA·DNA Concatamers by rolling-circle amplification as multivalent inhibitors of influenza A virus particles, ChemBioChem 20 (2019) 159–165, https://doi.org/10.1002/cbic.201800643.